The rhamnolipids of *Pseudomonas aeruginosa* change the mechanical properties of biogels

Maxime Deforet[1,*]

1. Sorbonne Université, Centre National de la Recherche Scientifique, Laboratoire Jean Perrin, LJP, Paris 75005, France;

∗ E-mail: maxime.deforet@sorbonne-universite.fr.

Keywords: *Pseudomonas aeruginosa, swarming, agar gel, surfactants, rhamnolipids*.

Abstract

Pseudomonas aeruginosa makes and secretes massive amounts of rhamnolipid surfactants that enable swarming motility over biogel surfaces. But how this rhamnolipids interact with biogels to assist swarming remains unclear. Here I use a combination of optical techniques across scales and genetically-engineered strains to demonstrate that rhamnolipids can induce agar gel swelling over distances >10,000x the body size of an individual cell. The swelling front is on the micrometric scale, and is easily visible using shadowgraphy. Rhamnolipid transport is not restricted to the surface of the gel, but occurs through the whole thickness of the plate and, consequently, the spreading dynamics depends on the local thickness. Surprisingly, rhamnolipids can cross the whole gel and induce swelling on the opposite side of a two-face Petri dish. The swelling front delimits an area where the mechanical properties of the surface properties are modified: water wets the surface more easily, which increases the motility of individual bacteria and enables collective motility. A genetically-engineered mutant unable to secrete rhamnolipids (*rhlA*$^-$), and therefore unable to swarm, is rescued from afar with rhamnolipids produced by a remote colony. These results exemplify the remarkable capacity of bacteria to change the physical environment around them.

Introduction

Bacteria have a remarkable ability to change the world around them through their collective behaviors [1, 2, 3]. Some of these changes are physical : bacteria interact mechanically with their environment [4] and they are also able to feedback on the physical environment [5, 6, 7].

Petri dishes with an agar biogel are widely used to investigate collective bacterial motility and its interplay with other biological processes [8]. This approach was used to uncover chemotactic genes [9, 10], mechanisms of action of pharmaceutical molecules [11], evolutionary dynamics [12], quorum sensing [13, 14], and other phenomenal collective behaviors of bacteria [15, 16, 17].

Agar gel serves as a physical and chemical substrate: cells are inoculated at the surface of the gel, they proliferate by consuming essential nutrients supplemented to the gel. In that regard, an agar plate is generally viewed as a passive element merely providing mechanical support, water, and nutrients. During colony growth, bacteria secrete osmolytes (exopolysaccharides), which draw water from the gel to equilibrate osmotic imbalance and contribute to colony swelling and expansion, in non-motile [18, 19] as well as in motile colonies [20, 21, 22]. While colony morphogenesis modeling attempts sometimes include nutrient and water depletion [23, 24], structural changes of agar gel are rarely considered.

In the case of the bacterium *Pseudomonas aeruginosa*, a common opportunistic pathogen, another gel modification needs to be considered: *P. aeruginosa* secretes rhamnolipids, a family of glycolipid surfactants of strong interest in medicine [25] and industry [26, 27], in particular for their antimicrobial properties, their capacity to emulsify oil and participate in bioremediation, and their good environmental compatibility and biodegradability. Secretion of rhamnolipids allows the colony to rapidly and collectively spread into a branched shape, a phenotype called swarming [28, 29]. Mutants that do not secrete rhamnolipids are unable to swarm [30, 31]. Due to their surfactant nature [32], rhamnolipids are often said to *lubricate the surface* [33], decrease *friction against the gel* [34], *act as a wetting agent* [35], or *lower surface tension* [20, 36]. But how the rhamnolipids interact with the agar biogel to enable swarming motility remains unclear.

Previous work used biophysical approaches to study how surfactant-assisted spreading of

liquid film can yield to branching. This has been explored on liquid and solid substrates [37, 38], and was extended to the case of *P. aeruginosa* swarming colonies [39, 40]. In those works, rhamnolipids were modeled as a thin film of insoluble surfactants secreted by the colony and diffusing at the surface of a gel. Differences of surfactant concentration inside and outside the colony yield to gradients of surface tension and induced a branching instability (Marangoni effect). Yet, rhamnolipids are soluble in water [41] and therefore are expected to diffuse though the agar gel, a hydrogel, whose structure could be modified through swelling [42, 43].

Here, I use a combination of imaging methods across scales to demonstrate that rhamnolipids secreted by the colony alter the physical properties of the agar gel, not only locally where they are secreted, but also all more widely around the bacteria. Moreover, their transport is not restricted to the surface. I find, instead, that the rhamnolipids imbibe the whole gel, which yields to gel swelling with a sharp swelling front. Bulk transport of rhamnolipids directly affects the expansion rate of the region imbibed by rhamnolipids. More generally, this is an example of the remarkable ability of bacteria to change the mechanical properties of the world surrounding them.

Results

Rhamnolipids cause biogel swelling

Wild-type *P. aeruginosa* colony spreads on soft agar by forming a branched colony, a behavior called swarming [29]. *rhlA*, a gene involved in production of rhamnolipids, is required for swarming: an *rhlA*$^-$ colony, which does not produce rhamnolipids, is unable to swarm (Figure 1A). Shadowgraphy, an optical method that reveals non-uniformities in transparent media by casting a shadow onto a white background [44], revealed that an area of the gel around the rhamnolipid-producing colony was modified: a thin darker line surrounded the colony (Figure 1B). Timelapse imaging confirmed this optical modification originated from the colony and propagates outward (See Movie 1). Since no modification emerged from an *rhlA*$^-$ colony, I hypothesized modification of the optical properties of the gel were due to secretion of rhamnolipids.

Rhamnolipids are secreted as a family of glycolipid molecules, made of one or two fatty acid chains (primarly 3-(3-hydroxyalkanoyloxy)alkanoic acid, HAA) associated with one or two rhamnose groups, called monorhamnolipids (mono-RLs) or dirhamnolipids (di-RLs) [45]. These molecules are lipids, therefore they could be localized using a lipid dye. Nile Red, whose emission spectrum depends on the polarity of the solvant [46], was mixed to the agar gel during gel preparation. Fluorescence microscopy confirmed a sharp drop of fluorescence intensity coincides with the location of the darker line visualized in shadowgraphy (Figure 1C). *rhlA*$^-$ colony does not produce HAA but still produces fatty acid chain precursors, whose lipid nature can be captured by Nile Red imaging. In this case, fluorescence intensity gradually varied with the distance to the colony, but no sharp transition was observed. I also measured the wetting property of the gel surface by performing sessile droplets experiments [47]. Water droplets were deposited on each side of the darker line localized by shadowgraphy. On average, the droplet footprint radius was 3.78 ± 0.27 (SD) mm on the colony side, and 2.13 ± 0.09 (SD) mm on the other side (Figure 1D). Neglecting gravity and therefore assuming a spherical cap shape allow the calculation of contact angles of 22.7^o and 35.6^o, respectively. The wetting footprint size was found to be uniform on the colony side, independent of the distance to the colony or the distance to the darker line. Similarly, the wetting footprint size was found to be uniform also outside the darker line. This confirms that the darker line marks a sharp limit of the rhamnolipid range, with surface properties that correlates with the presence of rhamnolipids.

To understand the origin of the darker line visible in shadowgraphy, I had to first evaluate its 3D profile. Using an optical profilometer (a device capable to measure 3D profile of a reflective surface with a nanometric resolution), I measured a jump of 8 µm, with a maximal slope of 3° (Figure 1E). The jump could emerge from two possible mechanisms: either it corresponds to a thick layer of rhamnolipid molecules covering the surface of the agar gel, as assumed by previous works [39, 40], or alternatively rhamnolipids infiltrate the gel and the jump corresponds to a gel swelling front. I embedded micrometric fluorescent beads during preparation of the gel and performed 3D-tracking to follow each bead while the line passed through the field of view. If rhamnolipids cover the gel surface, beads should not move. If rhamnolipids diffuse through

the gel and make it swell, beads should move up. Data shown in Figure 1F confirms a vertical movement of all the beads, synchronized with the passing line (see also Movie 2). The swelling amplitude was uniform across the first 50 µm (optical limitations of fluorescence microscopy hamper deeper observations). Of note, beads also moved laterally with a similar amplitude: they first moved outwards and then inwards (this corresponds to a dilatation wave, see Figure S1 for more details). This confirms rhamnolipids make the agar gel swell over large distances, and the darker line corresponds to a swelling front that is so steep that it can be seen by a naked eye and by shadowgraphy.

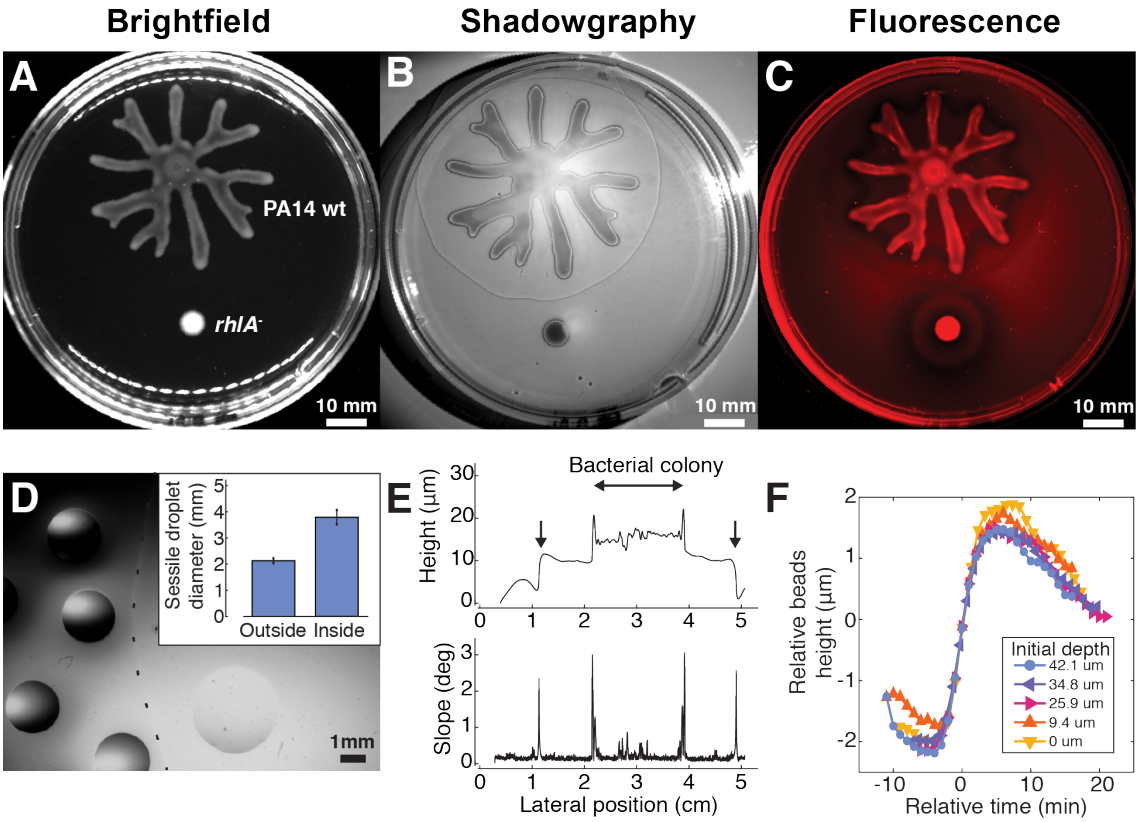

Figure 1: Rhamnolipids induce agar gel swelling. A-B-C: Wild-type *P. aeruginosa* and *rhlA*$^-$ colonies were grown on an agar gel. The former swarmed out and formed a branched colony, whereas the latter did not swarm. A: Brightfield image. B: Shadowgraphy image reveals a darker line (depicted by a black arrowhead) that corresponds to a swelling front. C: Fluorescence image, for Nile Red imaging, confirms the darker line correponds to a boundary of an area imbibed by rhamnolipids. D: An illustrative micrograph showing the sessile droplets experiments. Dashed line depicts the swelling front. The source colony is on the right side. Inset: comparison of the wetting footprint radius in the two conditions. Error bars are standard deviation. E: Top: a height profile of a gel, obtained from optical interferometry. Bottom: The local slope of the height profile. F: Vertical positions of fluorescent microbeads reveals gel swelling. The time axis for each trajectory is shifted using time synchronization from lateral displacement data (See Figure S1). Colors code for initial depth of each bead.

Rhamnolipids imbibe the bulk of the gel, not the surface

If transport of rhamnolipids is restricted to the gel surface, or if rhamnolipids diffuse through the gel following normal diffusion, their spreading rate should not depend on the local thickness of the gel. On the contrary, if Darcy's law governs rhamnolipids' transport, their spreading dynamics should depend on the local section of the gel. I used gels with varying thicknesses to test this hypothesis and check whether rhamnolipids imbibed the whole gel or only the upper part. First, I used gels with stepwise thickness. I placed a thick inert obstacle at the bottom surface of the Petri dish and poured the agar gel on top of them. The thickness of obstacles (1.5 mm) was chosen to be smaller than the gel thickness (3.5 mm) to make sure the upper surface remained flat. To simplify the geometry of the system and keep a local source of rhamnolipids, I inoculated a non-motile mutant (*flgK*$^-$) along a line. The swelling front coming out of the colony was found to propagate faster on top of obstacles (Figure 2A), where the gel section was smaller, and slower on top of thicker sections of the gel, which is compatible with a transport of rhamnolipids through the whole gel. This effect was also found in gels with gradual change of thickness. Pouring liquid agar on a tilted dish resulted in a gel with a spatial gradient of thickness: on this substrate, the swelling front advanced faster on the thinning side, slower on the thickening side, and at intermediate speed on the transverse directions (Figure 2B). Finally, I tested the swelling speed of gel of various thicknesses. Once again, thinner gels induced faster traveling speed of the swelling front (Figure 2C), in agreement with transport through the gel. Intriguingly, while thinner gels induce faster spreading of the swelling front, they also induce smaller swarming colonies (Figure S3). Colony did not swarm at all on plates lower than 7 mL. They gradually were larger and larger on thicker gels and the colony size was maximal on plates of the nominal volume (20 mL).

To further demonstrate transport of rhamnolipids through gels, I designed a "two-face" Petri dish. I inoculated bacteria on the lower side of the dish and a swelling front was observed on the upper side. The upper surface was characterized with shadowgraphy, profilometry, and sessile droplets (Figure 2D). These measurements confirmed that a rhamnolipid-induced swelling front

propagated to the upper surface, even though rhamnolipids were secreted from the lower surface.

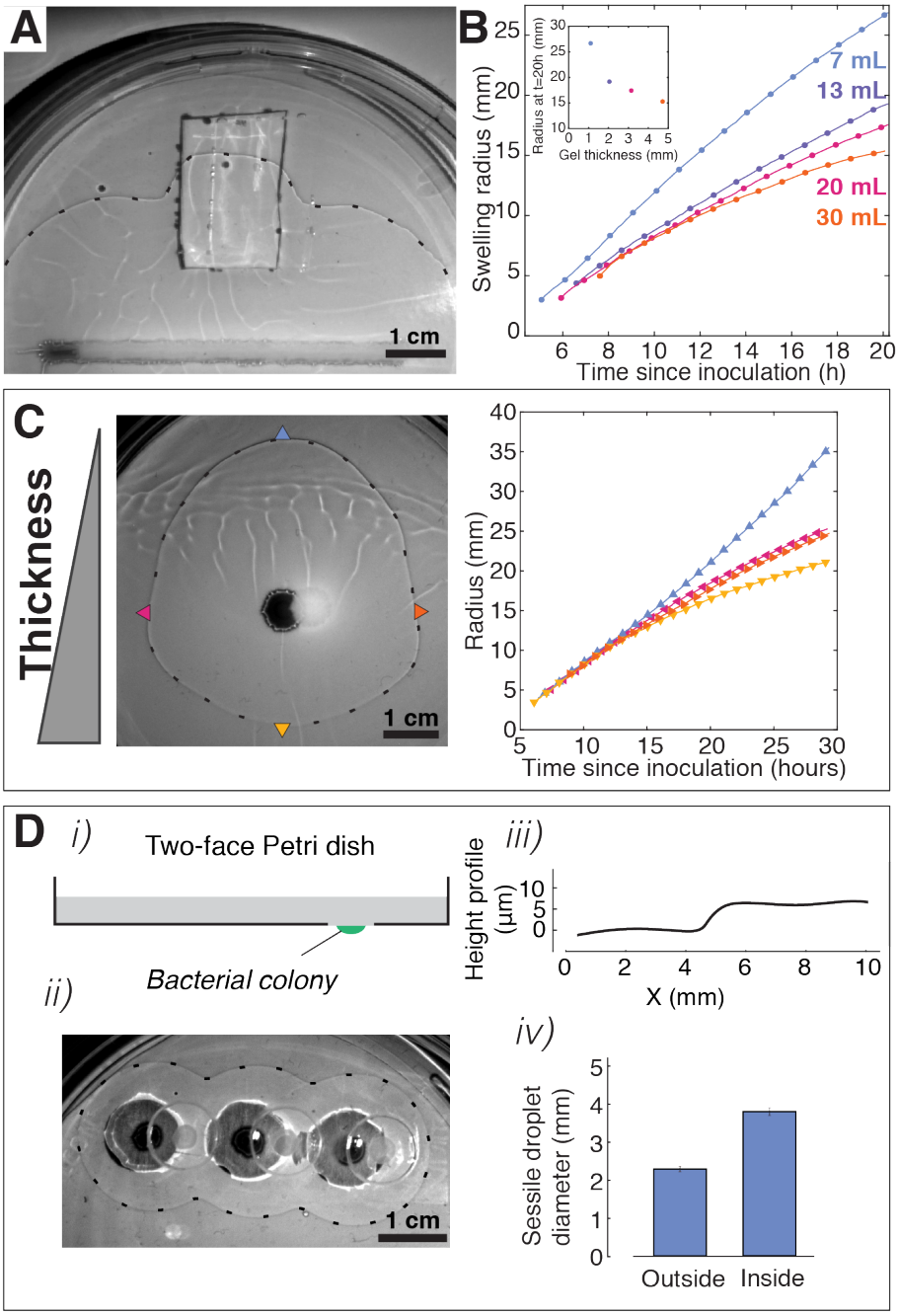

Figure 2: A: Image of the swelling front on a plate with an obstacle. The non-motile colony, inoculated along a line, is visible near the bottom of the image. B: Left: Image of the swelling front advancing on a tilted gel. Right: Positions of the swelling front as a function of time, for 4 locations depicted with arrowheads (top, bottom, left, and right). C: Positions of the swelling front as a function of time, for four plates with different thicknesses of gel. D: Two-face Petri dish confirms rhamnolipids spread through the gel. i) Schematic of a two-face Petri dish. ii) Shadowgraph of the swelling front emerging from three colonies, located on the other side of the gel. iii) Height profile obtained from optical profilometry. iv) Sessile droplet experiment confirms an significant difference in wetting property on either side of the swelling front. Error bars are standard deviation.

Rhamnolipids enable surface motility at the single-cell level

Rhamnolipids, transported within the gel, are required for the colony to spread at the surface of the gel. To better understand the interplay between bulk transport of rhamnolipids and surface motility, I used *rhlA*$^-$ mutant, which does not secrete rhamnolipids but is motile, as a sensor of ability to move on the gel as a function of presence of rhamnolipids. A wild-type colony was grown on agar gel and a small amount of planktonic *rhlA*$^-$ cells were seeded on the naked gel. Individual cells were found to be initially mostly non-motile. Motility was detected only in denser areas. The passage of the swelling front dramatically perturbed spatial organization of the cells (Figure 3A and Movie 3), and hampered direct comparison before/after. In particular, following individual cells was impossible. Instead, motility was assessed by coarse-grained image analysis (see Methods). The motility-density dependence was quantified and plotted against time (Figure 3B-C). Even though cells gradually became more motile with time, incoming rhamnolipids substantially increased cell motility, at all densities. Therefore, rhamnolipids are used by bacteria to alter their physical environment over large distances and enable surface motility.

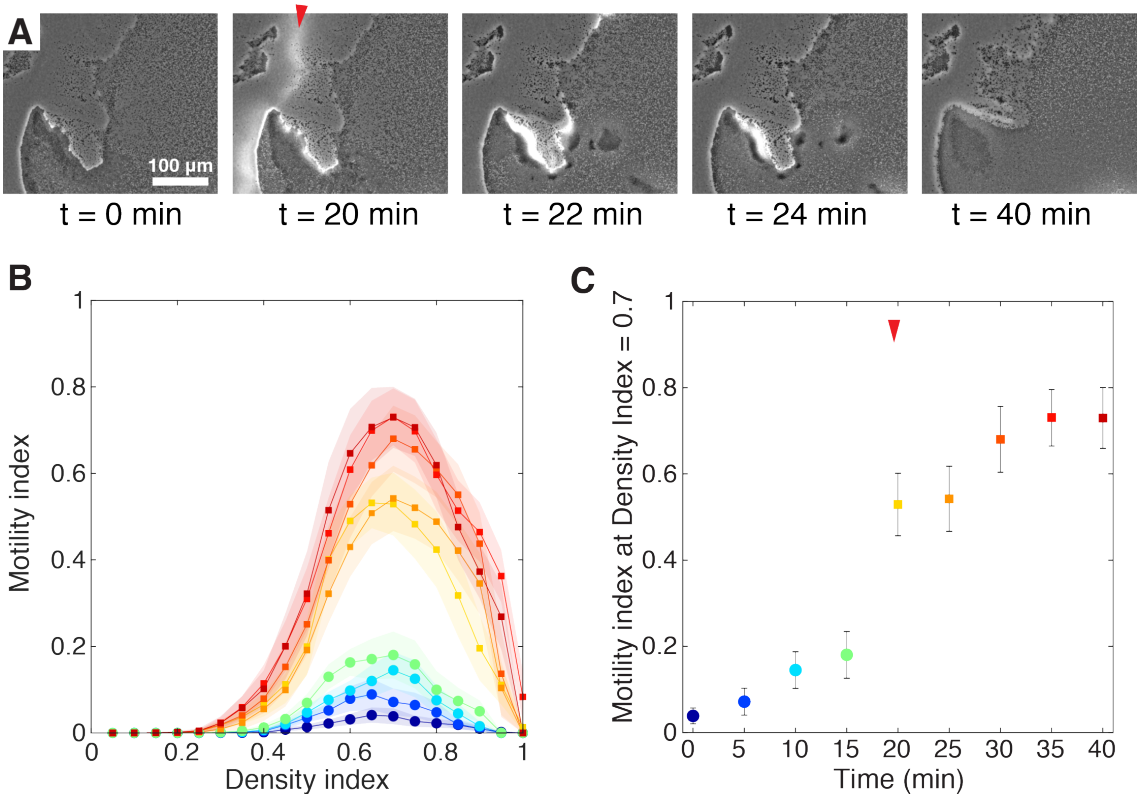

Figure 3: A: Snapshots of micrographs showing *rhlA*$^-$ cells before and after the swelling front passed through. A red arrowhead depicts the swelling front, visible as a white halo in phase contrast imaging, and moving from the left to the right of the field of view. B: Motility-density analysis reveals rhamnolipids greatly facilitate single-cell motility. Color code is defined in panel C (one curve every 5 minutes). Shading represents standard deviations. C: The effect of rhamnolipids on motility is abrupt, and corresponds to the passage of the swelling front (depicted by the red arrowhead). Error bars represent standard deviations.

Swarming rescue experiments confirm rhamnolipids diffuse across the biogel

This microscopic-scale rescue of motility *rhlA*$^-$ mutants inspired me to test if such distant rescue could occur at a macroscopic scale. A plate was inoculated with wild-type cells on one side, and with *rhlA*$^-$ cells on the other side. As already showed in Figure 1, the wild-type colony secretes rhamnolipids (inducing a swelling front) and swarms into a branched shape. The *rhlA*$^-$ colony does not secrete rhamnolipids and does not swarm. However, wild-type colony spreading closely follows the swelling front. To avoid the *rhlA*$^-$ colony from being reached by the expanding wild-type colony before it started swarming, I turned into a mutant over-producer of rhamnolipids: *rhlA*$^-$ *pBAD-RhlAB*, whose rhamnolipid promoter expression is induced by a chemical cue, L-arabinose. The *rhlA*$^-$ *pBAD-RhlAB* colony dedicates a large part of its metabolism to rhamnolipid secretion rather than cell proliferation, which yields to a faster swelling front and a slower colony spreading. As shown on Figure 4A (and Movie 5), *rhlA*$^-$ colonies started swarming a few hours after the swelling front reached it.

I reproduced the rescue experiment on a two-face Petri dish, with the over-producing colony (*rhlA*$^-$ *pBAD-RhlAB*) on one side and *rhlA*$^-$ on the other side (Figure 4B, Movie 5). This confirms rhamnolipids imbibe the whole gel, physically alter the gel over large distance, and control colony morphogenesis even on the opposite surface.

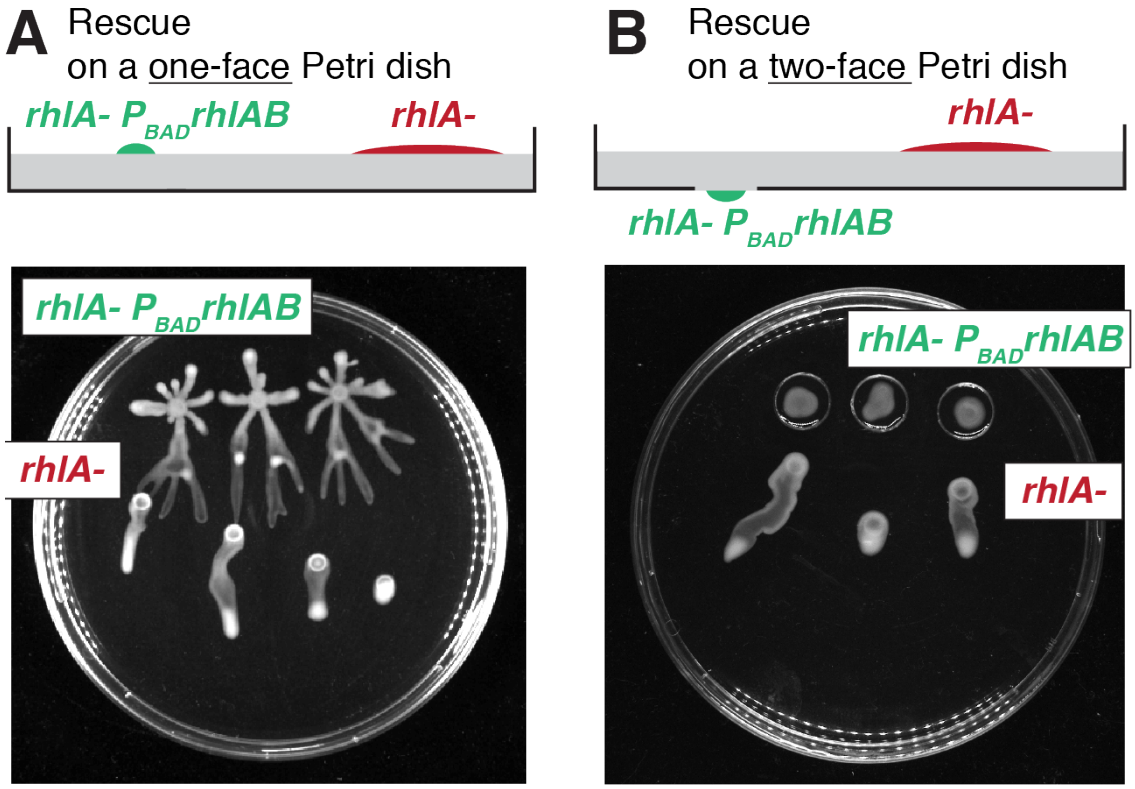

Figure 4: Swarming rescue experiments. A: On one-face Petri dish, *rhlA*$^-$ *pBAD-RhlAB* and *rhlA*$^-$ colonies are grown on the same side. B: On two-face Petri dish, *rhlA*$^-$ *pBAD-RhlAB* are grown on one side (within the small hole) and *rhlA*$^-$ are grown on the opposite side. Control experiment results (with *rhlA*$^-$ instead of *rhlA*$^-$ *pBAD-RhlAB*) are provided in Supplementary Figure S2. Snapshots are taken 18 hours after inoculation. Timelapse videos of the rescue experiments are available in Movie 5.

Physical alteration of the gel by rhamnolipids correlates with colony shape

Since *P. aeruginosa* is capable to alter physical properties of its environment over long distances, I wanted to verify whether this would hold true for a range of environments. I used agar gels of various agar concentrations (0.4%, 0.5%, 0.6%, and 0.7%) to simulate environments of different physical properties. Agar gel elastic modulus and pore size were previously characterized and they were found to be highly dependent on agar concentration. From the literature, pore size varies from 400 nm at 0.4% to 100 nm at 0.7% [48, 49]; elastic modulus varies from 4 kPa at 0.4% to 18 kPa at 0.7% [50, 51]. (Most studies focused on agarose, a polysaccharide isolated from agar, but with comparable mechanical properties; rheological measurements are difficult to perform on these soft gels, and those figures must be taken with a grain of salt.)

I grew *P. aeruginosa* on plates at the four agar concentrations and confirmed a result already described: swarming colony morphogenesis is highly dependent on the gel properties (Figure 5A). At low concentration (0.4%), the colony was smaller and more circular than the branch colony formed at 0.5%. At 0.6%, the colony was still branched but smaller than 0.5% colony. The 0.7% colony did not spread at all. Following the same trend, macroscopic swarming rescue on two-face Petri dished occurred similarly at 0.4% and 0.5%, little spreading was visible at 0.6%, and no spreading at all at 0.7% (Figure 5B). In parallel, I characterized the gel and its alteration by secreted rhamnolipids, for the four agar concentrations.

First, I reproduced the sessile droplet experiment as in Figure 1D. Footprint diameters increased with gel concentration when droplets were deposited on the raw gel surface (outside the rhamnolipid imbibed area), from 1.77 ± 0.13 mm for 0.4% to 2.41 ± 0.10 mm for 0.7% (Figure 5C). In contrast, when droplets were deposited inside the rhamnolipids-imbibed area, footprint diameters were overall much greater and independent of agar concentrations. They were about 3.86 ($\pm$0.27 mm) for all conditions, as if rhamnolipids equalized the wetting properties of the imbibed gels.

Second, I measured the swelling front height profiles generated by rhamnolipid imbibition (Figure 5D). I observed a strong influence of agar concentration: the swelling front jump (mea-

sured 1 mm away from the front, see details in Methods) was 27.4 ± 4.2 µm for 0.4% and gradually decreased for larger agar concentrations (3.9 ± 1.8 µm for 0.7%). This trend was confirmed by shadowgraphy, a contrast imaging method that relies on non-uniformities deviating light rays: the front on a 0.4% gel yielded to a strongly contrasted black line, whereas the front on a 0.7% gel was nearly not visible.

Third, I located the position of the swelling front as a function of time, on two-face Petri dishes. An *rhlA*$^-$ *pBAD-RhlAB* colony was seeded on the small aperture on the opposite side, in order to limit the spatial expansion of the rhamnolipid source and to allow for comparison of swelling front advancing speeds across agar concentrations without having to control for the source colony size. The position of the swelling front followed a power law $r = t^{\alpha}$ with α ranging between 0.4 and and 0.6 (Figure 5D, inset), in agreement with imbibition processes [52]. However, a reproducible estimation of the exponent was difficult, considering the day-to-day variability of agar gel preparation previously described [53, 54]. I turned to a simpler and more robust quantification: the position of the front 15 hours after inoculation. Using this measure, I found that the swelling front advanced significantly faster in low concentration agar gels compared to high concentration agar gels (Figure 5E).

Taken together, these results demonstrate that swarming colony morphogenesis correlates with the long distance physical alteration of the gel, across a range of agar concentrations.

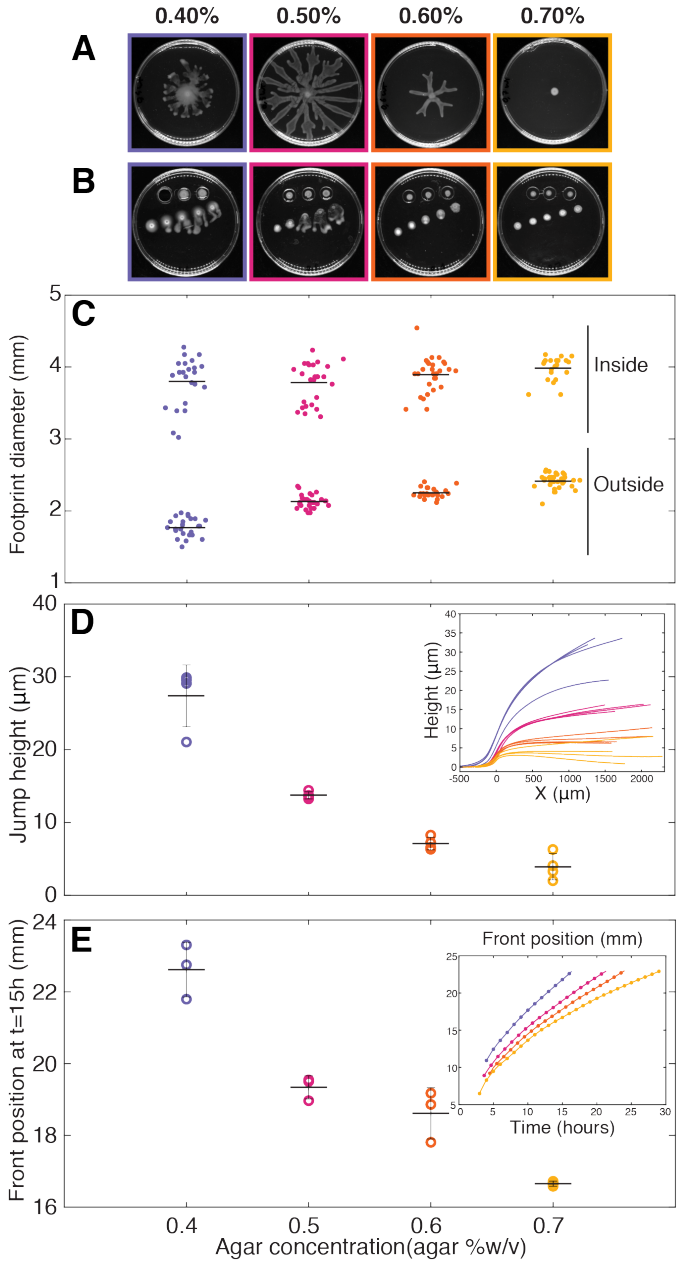

Figure 5: Physical alteration of the gel occurs across a range of agar concentration. A: Snapshots of *P. aeruginosa* swarming colonies, 22 hours after inoculation. Each snapshot is surrounded by a square whose color consistently represents the agar concentration across panels. B: Snapshots of macroscopic rescue experiments, 22 hours after inoculation. (Note one agar patch fell from the two-face Petri dish on the 0.4% plate, just before image acquisition.) C: Footprint diameters for sessile droplet experiments. Droplets were deposited within the rhamnolipid-imbibed area (denoted "Inside") or outside the swelling front (denoted "Outside"). Data points positions were randomized on the horizontal axis for better visualization. Data points originates from 2 biological replicates. D: Jump height measured 1 mm from the swelling front. Inset: Height profiles obtained by optical interferometry. E: Position of the swelling front 15 hours after inoculation. Data points originates from 3 technical replicates. Inset: Time evolution of the front position, from one replicate. For all panels, horizontal bars are dataset averages and vertical bars are standard deviations.

Discussion

Here, I documented that rhamnolipids physically modify the agar gel by inducing a gel swelling. The swelling front displays a maximum angle of 3° that is sufficient to make the edge visible to the naked eye and by shadowgraphy. Previous work had already noted a change of the surface visual aspect. Those studies used terms like "zone of fluid", "zone of liquid" [30], or "ring of biosurfactants" [31] to describe this modified surface state, but my findings show those views were incomplete.

Furthermore, I demonstrated that transport of rhamnolipids is not restricted to the surface of the agar gel. On the contrary, rhamnolipids imbibe the whole thickness of the gel. A direct consequence of the transport in volume is that spreading speed depends on the local section of the gel, with faster spreading on thinner gels. The modulation of the swelling front traveling speed is likely to be conflated with resource availability: a thinner gel contains less nutrient, yields to a smaller colony, and is expected to produce to a slower swelling front. Experimental data goes in the opposite direction: thinner gels yields to faster, not slower, swelling front. Interestingly, colonies do not spread faster on thinner gel. This highlights the complex interplay between resources availability, rhamnolipids spatial distribution, and swarming motility [31, 33].

The swelling front advancing speed, typically 1 mm/h, is substantially lower than the spreading dynamics of surfactants on liquid films (typically 1 mm/s [37]). It resembles precursor front in fluid imbibition dynamics of porous materials, which can be interpreted as non-Fickian transport in a Darcy flow [52]. Moreover, the deformation of the agar gel is likely to be coupled to the effective diffusivity of rhamnolipids through the gel. Since rhamnolipids are capable to reach the opposite surface, one could assume, in first approximation, a uniform concentration profile across the gel thickness. Yet, agar gel is a physically-crosslinked hydrogel, and the physicochemistry of its interaction with surfactants could lead to a non-uniform profile of concentration [47, 55].

Alteration of the biotic or abiotic environment by living organisms have the potential to modulate motility and dispersal mechanics. Secreted metabolites can act as chemoattractants [56,

57], trigger quorum sensing [58], participate in self-organization in stigmergic behavior [59, 60], and control single-cell motility [61]. These mechanisms rely on release of diffusible molecules, or local deposition of non-diffusible signals. Here, I evidenced a mechanism where bacteria alter their physical world on a lengthscale substantially larger that their own size. I confirmed this effect holds true across a range of agar concentration. It would be interesting to test other biogel materials [62], especially those with biomedical implications, such as mucus [63, 64].

The complex interplay between surfactants, biogel substrate and bacterial motility that I unveiled here highlights the intricate physical phenomena underlying swarming motility. More generally, it sheds a new light on interactions between bacteria and the tri-dimensional environment that surrounds them: a unique example of the capacity of bacteria to change the mechanical properties of the world around them.

Methods

Bacterial strains and growth conditions The bacterial strains used in this study are described in Table S1. Bacterial cells were routinely grown in LB at 37ºC with aeration. Swarming plates were prepared as previously described [31]. Agar concentration, unless specified otherwise, is 0.5 % (w/v). Overnight culture of bacteria were washed twice in PBS and 2 µL of the washed suspension were used to inoculate a swarming plate in the center. The plates were then flipped and placed inside a 37ºC microbiological incubator. *rhlA*$^-$ *pBAD-RhlAB* colonies were grown on 1% L-arabinose swarming plates to induce expression of the *rhlA* gene and robust secretion of rhamnolipids.

Whole swarming colony An automated device was built inside a microbiological incubator (Heratherm IGS 100, ThermoFisher Scientific), for fluorescence, shadowgraphy, and brighfield imaging of a 10-cm diameter Petri dish. A LED light source (pE-4000, Coolled, UK) was used for fluorescence excitation. A set of lenses and mirrors were used to bring an even illumination pattern onto the plate. A single LED light source (Thorlabs, USA) was positioned on one side of the chamber for shadowgraphy imaging. Generic white LED strings (Mouser, France) were

positioned above the plate for brightfield imaging. Images were acquired with a CMOS camera (Cellcam Centro, Cairn Research, UK) with a macro lens (Navitar MVL7000, Thorlabs, USA). A dual-band emission filter (59010m, Chroma, USA) was mounted between the camera and the lens, for green and red fluorescence imaging. All devices were controlled with µManager (http://www.micro-manager.org).

Sessile droplets Plates and swarming colonies were prepared as explained above. Plates were taken out of the incubator and placed under a Axiozoom V16 macroscope (Zeiss), set at the lowest magnification (field of view is 25.7x21.5mm), equipped with a CMOS camera (BlackFly S, FLIR, USA), and illuminated through a transilluminator (Zeiss) with a mirror position that mimics DIC illumination. 1 µL droplets of swarming media (recipe identical to that of the swarming plate, but without agar) were deposited on the surface of the gel, either inside or outside the swelling front generated by the colony. A movie was recorded as tens of droplets were deposited. Footprint diameters were measured, immediately after deposition, using ImageJ.

Fluorescent bead tracking For quantifying gel swelling, 1 µm fluorescent polysterene beads (F13083, ThermoFisher Scientific) were added during the swarming plate preparation (final concentration of 10^5 beads/mL). Colony were grown inside a microscopy incubator (Oko-Lab, Italy), mounted an a IX-81 Olympus inverted microscope, equipped with a LED light source (pE-4000, Coolled, UK). Images were taken with a 20x objective and a CMOS camera (BlackFly S, FLIR, USA), every minute, for 30 minutes, while the swelling front was passing through the field of view (confirmed by phase-contrast imaging). Diffraction pattern detection, beads detection, tracking, and calculation of the vertical displacement were performed with custom-made routines in MATLAB (MathWorks, USA). Calibration between diffraction pattern radius and vertical position was done by taking a vertical stack of images.

Profilometry Height profiles were measured with a Zegage Pro interferometry profilometer (Zygo) equipped with a 5x Michelson objective (Nikon). An acquisition took 5 seconds (for one field of view 2x2.7 mm), and 20 positions were stitched together to reconstruct the whole

height profile (Figure 1E). For Figure 5C, the profiles were measured when the diameter of the rhamnolipids-imbibed area was approximately 3 cm in diameter. Four positions were recorded per plate (the 4th roots of unity). Each profile was then measured perpendicularly to the swelling front. The $X = 0$ location was identified as the inflection point of the profile. The reference height $Z = 0$ was imposed at location $X = -500$ µm and $X = -400$ µm, which tilt-corrected the whole profile. Heights in Figure 5C were measured at $X = 1000$ µm.

Stepwise substrate A 1.5 mm thick sheet of polydimethylsiloxane (PDMS) was made following standard protocol (RTV615A+B, 10:1, Momentive Performance Materials). A 1x2 cm slab was cut out of the PDMS sheet and was placed in a Petri dish. 20 mL of agar gel was then poured on top of the substrate, following usual swarming plate protocol.

Two-face Petri dish The bottom of a Petri dish was drilled with a 10-mm drill bit. Holes were deburred with a 13-mm drill bit. Dishes were sterilized in 70% ethanol. The bottom side of each hole was taped with a piece of Parafilm, which was peeled off after the agar gel was poured and solidified.

Single-cell motility A suspension of *rhlA*$^-$ cells growing in liquid swarming media was spun down. A 20 µL plastic pipette tip was used to sample cells from the pellet and to transfer cells onto the gel surface (approximately 2 mm from the swelling front identified in shadowgraphy). One second videos (46 frames-per-second) were acquired every 5 minutes, at 10x magnification, in phase contrast, with an IX-81 Olympus inverted microscope. Auto-focus was performed before each acquisition. Image analysis was performed independently for each video: Local density was measured on the first frame of the video, by thresholding the phase-contrast image, followed by local averaging. The Density Index, defined to be between 0 (no cell) and 1 (cells form a uniformly dark population) is therefore the proportion of neighboring pixels that contains cells. To evaluate motility, the difference between the maximum projection and the minimum projection across the time-stack yields to a map where pixels were bright if their grey values changed during the video. Then, a threshold was applied and the result was locally average to produce a map of

Speed Index between 0 (no pixel change) and 1 (all pixels have change values). This coarse-grained quantification is valid as long as cells are not too dense and cells do not move too much during one video (therefore, the analysis was limited to the region of the field of view where cells did not pile up and only one-second long videos were considered). To check the robustness of the method, various thresholding values have been tried, without significantly affecting the results.

Acknowledgments

I thank members of the Laboratoire Jean Perrin for fruitful discussions. I am grateful to Françoise Brochard-Wyart for pointing me to the reference [52]. This project has received financial support from the CNRS through the MITI interdisciplinary program, and from the Alliance Sorbonne Université through the Emergence program.

References

[1] Kai Papenfort and Bonnie L Bassler. Quorum sensing signal–response systems in gram-negative bacteria. *Nature Reviews Microbiology*, 14(9):576–588, 2016.

[2] Despoina AI Mavridou, Diego Gonzalez, Wook Kim, Stuart A West, and Kevin R Foster. Bacteria use collective behavior to generate diverse combat strategies. *Current Biology*, 28(3):345–355, 2018.

[3] Christoph Ratzke and Jeff Gore. Modifying and reacting to the environmental ph can drive bacterial interactions. *PLoS biology*, 16(3):e2004248, 2018.

[4] Alexandre Persat, Carey D Nadell, Minyoung Kevin Kim, Francois Ingremeau, Albert Siryaporn, Knut Drescher, Ned S Wingreen, Bonnie L Bassler, Zemer Gitai, and Howard A Stone. The mechanical world of bacteria. *Cell*, 161(5):988–997, 2015.

[5] Veysel Berk, Jiunn CN Fong, Graham T Dempsey, Omer N Develioglu, Xiaowei Zhuang, Jan Liphardt, Fitnat H Yildiz, and Steven Chu. Molecular architecture and assembly principles of vibrio cholerae biofilms. *Science*, 337(6091):236–239, 2012.

[6] Su Chuen Chew, Binu Kundukad, Thomas Seviour, Johan RC Van der Maarel, Liang Yang, Scott A Rice, Patrick Doyle, and Staffan Kjelleberg. Dynamic remodeling of microbial biofilms by functionally distinct exopolysaccharides. *MBio*, 5(4):e01536–14, 2014.

[7] Carolina Tropini. How the physical environment shapes the microbiota. *Msystems*, 6(4):e00675–21, 2021.

[8] Navish Wadhwa and Howard C Berg. Bacterial motility: machinery and mechanisms. *Nature Reviews Microbiology*, pages 1–13, 2021.

[9] Derek Greenfield, Ann L McEvoy, Hari Shroff, Gavin E Crooks, Ned S Wingreen, Eric Betzig, and Jan Liphardt. Self-organization of the escherichia coli chemotaxis network imaged with super-resolution light microscopy. *PLoS biology*, 7(6):e1000137, 2009.

[10] Remy Colin, Bin Ni, Leanid Laganenka, and Victor Sourjik. Multiple functions of flagellar motility and chemotaxis in bacterial physiology. *FEMS Microbiology Reviews*, 45(6):fuab038, 2021.

[11] OK Mirzoeva, RN Grishanin, and PC Calder. Antimicrobial action of propolis and some of its components: the effects on growth, membrane potential and motility of bacteria. *Microbiological research*, 152(3):239–246, 1997.

[12] Michael Baym, Tami D Lieberman, Eric D Kelsic, Remy Chait, Rotem Gross, Idan Yelin, and Roy Kishony. Spatiotemporal microbial evolution on antibiotic landscapes. *Science*, 353(6304):1147–1151, 2016.

[13] Ruth Daniels, Jos Vanderleyden, and Jan Michiels. Quorum sensing and swarming migration in bacteria. *FEMS microbiology reviews*, 28(3):261–289, 2004.

[14] Nachiket G Kamatkar and Joshua D Shrout. Surface hardness impairment of quorum sensing and swarming for pseudomonas aeruginosa. *PloS one*, 6(6):e20888, 2011.

[15] Hannah Jeckel, Eric Jelli, Raimo Hartmann, Praveen K Singh, Rachel Mok, Jan Frederik Totz, Lucia Vidakovic, Bruno Eckhardt, Jörn Dunkel, and Knut Drescher. Learning the space-time phase diagram of bacterial swarm expansion. *Proceedings of the National Academy of Sciences*, 116(5):1489–1494, 2019.

[16] Divakar Badal, Abhijith Vimal Jayarani, Mohammad Ameen Kollaran, Deep Prakash, Monisha P, Varsha Singh, and Joanna B. Goldberg. Foraging signals promote swarming in starving pseudomonas aeruginosa. *mBio*, 0(0):e02033–21, 2021.

[17] Hilary Monaco, Kevin S Liu, Tiago Sereno, Maxime Deforet, Bradford P Taylor, Yanyan Chen, Caleb C Reagor, and Joao B Xavier. Spatial-temporal dynamics of a microbial cooperative behavior resistant to cheating. *Nature communications*, 13(1):1–11, 2022.

[18] Gabriel E Dilanji, Max Teplitski, and Stephen J Hagen. Entropy-driven motility of sinorhizobium meliloti on a semi-solid surface. *Proceedings of the Royal Society B: Biological Sciences*, 281(1784):20132575, 2014.

[19] Agnese Seminara, Thomas E Angelini, James N Wilking, Hera Vlamakis, Senan Ebrahim, Roberto Kolter, David A Weitz, and Michael P Brenner. Osmotic spreading of bacillus subtilis biofilms driven by an extracellular matrix. *Proceedings of the National Academy of Sciences*, 109(4):1116–1121, 2012.

[20] Alexander Yang, Wai Shing Tang, Tieyan Si, and Jay X. Tang. Influence of physical effects on the swarming motility of pseudomonas aeruginosa. *Biophysical Journal*, 112(7):1462–1471, 2017.

[21] Hui Ma, Jordan Bell, Weijie Chen, Sridhar Mani, and Jay X Tang. An expanding bacterial colony forms a depletion zone with growing droplets. *Soft Matter*, 17(8):2315–2326, 2021.

[22] Ben Rhodeland, Kentaro Hoeger, and Tristan Ursell. Bacterial surface motility is modulated by colony-scale flow and granular jamming. *Journal of the Royal Society Interface*, 17(167):20200147, 2020.

[23] Siddarth Srinivasan, C Nadir Kaplan, and L Mahadevan. A multiphase theory for spreading microbial swarms and films. *Elife*, 8:e42697, 2019.

[24] Jing Yan, Carey D Nadell, Howard A Stone, Ned S Wingreen, and Bonnie L Bassler. Extracellular-matrix-mediated osmotic pressure drives vibrio cholerae biofilm expansion and cheater exclusion. *Nature communications*, 8(1):1–11, 2017.

[25] Priyanka Thakur, Neeraj K Saini, Vijay Kumar Thakur, Vijai Kumar Gupta, Reena V Saini, and Adesh K Saini. Rhamnolipid the glycolipid biosurfactant: Emerging trends and promising strategies in the field of biotechnology and biomedicine. *Microbial Cell Factories*, 20(1):1–15, 2021.

[26] A Varvaresou and K Iakovou. Biosurfactants in cosmetics and biopharmaceuticals. *Letters in applied microbiology*, 61(3):214–223, 2015.

[27] Eduardo J Gudiña, Ana I Rodrigues, Eliana Alves, M Rosário Domingues, José A Teixeira, and Lígia R Rodrigues. Bioconversion of agro-industrial by-products in rhamnolipids

toward applications in enhanced oil recovery and bioremediation. *Bioresource technology*, 177:87–93, 2015.

[28] Matthew F Copeland and Douglas B Weibel. Bacterial swarming: a model system for studying dynamic self-assembly. *Soft matter*, 5(6):1174–1187, 2009.

[29] Daniel B Kearns. A field guide to bacterial swarming motility. *Nature Reviews Microbiology*, 8(9):634–644, 2010.

[30] Nicky C. Caiazza, Robert M. Q. Shanks, and G. A. O'Toole. Rhamnolipids modulate swarming motility patterns of ¡i¿pseudomonas aeruginosa¡/i¿. *Journal of Bacteriology*, 187(21):7351–7361, 2005.

[31] Joao B Xavier, Wook Kim, and Kevin R Foster. A molecular mechanism that stabilizes cooperative secretions in pseudomonas aeruginosa. *Molecular microbiology*, 79(1):166–179, 2011.

[32] Judy Q Yang, Joseph E Sanfilippo, Niki Abbasi, Zemer Gitai, Bonnie L Bassler, and Howard A Stone. Evidence for biosurfactant-induced flow in corners and bacterial spreading in unsaturated porous media. *Proceedings of the National Academy of Sciences*, 118(38):e2111060118, 2021.

[33] Kerry E Boyle, Hilary Monaco, Dave van Ditmarsch, Maxime Deforet, and Joao B Xavier. Integration of metabolic and quorum sensing signals governing the decision to cooperate in a bacterial social trait. *PLoS computational biology*, 11(6):e1004279, 2015.

[34] Theresa Hölscher and Ákos T Kovács. Sliding on the surface: bacterial spreading without an active motor. *Environmental Microbiology*, 19(7):2537–2545, 2017.

[35] Julien Tremblay, Anne-Pascale Richardson, François Lépine, and Eric Déziel. Self-produced extracellular stimuli modulate the pseudomonas aeruginosa swarming motility behaviour. *Environmental Microbiology*, 9(10):2622–2630, 2007.

[36] Sina Rütschlin and Thomas Böttcher. Inhibitors of bacterial swarming behavior. *Chemistry–A European Journal*, 26(5):964–979, 2020.

[37] Omar K Matar and Sandra M Troian. The development of transient fingering patterns during the spreading of surfactant coated films. *Physics of Fluids*, 11(11):3232–3246, 1999.

[38] Omar K Matar and Richard V Craster. Dynamics of surfactant-assisted spreading. *Soft Matter*, 5(20):3801–3809, 2009.

[39] Maarten Fauvart, P Phillips, D Bachaspatimayum, Natalie Verstraeten, Jan Fransaer, Jan Michiels, and Jan Vermant. Surface tension gradient control of bacterial swarming in colonies of pseudomonas aeruginosa. *Soft Matter*, 8(1):70–76, 2012.

[40] Sarah Trinschek, Karin John, and Uwe Thiele. Modelling of surfactant-driven front instabilities in spreading bacterial colonies. *Soft Matter*, 14(22):4464–4476, 2018.

[41] Ahmad Mohammad Abdel-Mawgoud, Mohammad Mabrouk Aboulwafa, and Nadia Abdel-Haleem Hassouna. Characterization of rhamnolipid produced by pseudomonas aeruginosa isolate bs20. *Applied biochemistry and biotechnology*, 157(2):329–345, 2009.

[42] Azeem Bibi, Sadiq-ur Rehman, Rashida Faiz, Tasleem Akhtar, Mohsan Nawaz, and Saira Bibi. Effect of surfactants on swelling capacity and kinetics of alginate-chitosan/cnts hydrogel. *Materials Research Express*, 6(8):085065, 2019.

[43] Siyuan Li, Mengxue Zhang, and Bryan D Vogt. Delayed swelling and dissolution of hydrophobically associated hydrogel coatings by dilute aqueous surfactants. *ACS Applied Polymer Materials*, 4(1):250–259, 2021.

[44] Gary S Settles. *Schlieren and shadowgraph techniques: visualizing phenomena in transparent media*. Springer Science & Business Media, 2001.

[45] Merced Gutierrez, Mun Hwan Choi, Baoxia Tian, Ju Xu, Jong Kook Rho, Myeong Ok Kim, You-Hee Cho, and Sung Chul Yoon. Simultaneous inhibition of rhamnolipid and poly-

hydroxyalkanoic acid synthesis and biofilm formation in pseudomonas aeruginosa by 2-bromoalkanoic acids: Effect of inhibitor alkyl-chain-length. *PLOS ONE*, 8(9):1–11, 09 2013.

[46] Wulin Teo, Andrew V. Caprariello, Megan L. Morgan, Antonio Luchicchi, Geert J. Schenk, Jeffrey T. Joseph, Jeroen J. G. Geurts, and Peter K. Stys. Nile red fluorescence spectroscopy reports early physicochemical changes in myelin with high sensitivity. *Proceedings of the National Academy of Sciences*, 118(8):e2016897118, 2021.

[47] Mehdi Banaha, Adrian Daerr, and Laurent Limat. Spreading of liquid drops on agar gels. *The European Physical Journal Special Topics*, 166(1):185–188, 2009.

[48] Janaky Narayanan, Jun-Ying Xiong, and Xiang-Yang Liu. Determination of agarose gel pore size: Absorbance measurements vis a vis other techniques. In *Journal of Physics: Conference Series*, volume 28, page 017. IOP Publishing, 2006.

[49] Nicholas L Cuccia, Suraj Pothineni, Brady Wu, Joshua Méndez Harper, and Justin C Burton. Pore-size dependence and slow relaxation of hydrogel friction on smooth surfaces. *Proceedings of the National Academy of Sciences*, 117(21):11247–11256, 2020.

[50] Jean-Michel Guenet and Cyrille Rochas. Agarose sols and gels revisited. In *Macromolecular symposia*, volume 242, pages 65–70. Wiley Online Library, 2006.

[51] Bosi Mao, Thibaut Divoux, and Patrick Snabre. Normal force controlled rheology applied to agar gelation. *Journal of Rheology*, 60(3):473–489, 2016.

[52] Eduardo N de Azevedo, Lars R Alme, M Engelsberg, Jon Otto Fossum, and Paul Dommersnes. Fluid imbibition in paper fibers: Precursor front. *Physical Review E*, 78(6):066317, 2008.

[53] Dae-Gon Ha, Sherry L Kuchma, and George A O'Toole. Plate-based assay for swarming motility in pseudomonas aeruginosa. In *Pseudomonas methods and protocols*, pages 67–72. Springer, 2014.

[54] Melanie M Pearson. Methods for studying swarming and swimming motility. In *Proteus mirabilis*, pages 15–25. Springer, 2019.

[55] Shilpi Boral, Anita Saxena, and HB Bohidar. Syneresis in agar hydrogels. *International journal of biological macromolecules*, 46(2):232–236, 2010.

[56] Evanthia T Roussos, John S Condeelis, and Antonia Patsialou. Chemotaxis in cancer. *Nature Reviews Cancer*, 11(8):573–587, 2011.

[57] Remy Colin and Victor Sourjik. Emergent properties of bacterial chemotaxis pathway. *Current opinion in microbiology*, 39:24–33, 2017.

[58] Christopher M Waters, Bonnie L Bassler, et al. Quorum sensing: cell-to-cell communication in bacteria. *Annual review of cell and developmental biology*, 21(1):319–346, 2005.

[59] Guy Theraulaz and Eric Bonabeau. A brief history of stigmergy. *Artificial life*, 5(2):97–116, 1999.

[60] Joseph D'alessandro, Victor Cellerin, Olivier Benichou, René Marc Mège, Raphaël Voituriez, Benoît Ladoux, et al. Cell migration guided by long-lived spatial memory. *Nature Communications*, 12(1):1–10, 2021.

[61] Esther Wershof, Danielle Park, Robert P Jenkins, David J Barry, Erik Sahai, and Paul A Bates. Matrix feedback enables diverse higher-order patterning of the extracellular matrix. *PLoS computational biology*, 15(10):e1007251, 2019.

[62] Charles D Morin and Eric Déziel. Use of alternative gelling agents reveals the role of rhamnolipids in pseudomonas aeruginosa surface motility. *Biomolecules*, 11(10):1468, 2021.

[63] Amy TY Yeung, Alicia Parayno, and Robert EW Hancock. Mucin promotes rapid surface motility in pseudomonas aeruginosa. *MBio*, 3(3):e00073–12, 2012.

[64] Tamara Rossy, Tania Distler, Joern Pezoldt, Jaemin Kim, Lorenzo Tala, Nikolaos Bouklas, Bart Deplancke, and Alexandre Persat. Pseudomonas aeruginosa contracts mucus to rapidly form biofilms in tissue-engineered human airways. *bioRxiv*, 2022.

[65] Milton N Schroth, John J Cho, Sylvia K Green, Spyros D Kominos, et al. Epidemiology of pseudomonas aeruginosa in agricultural areas. *Journal of Medical Microbiology*, 67(8):1191–1201, 2018.

[66] George A O'Toole and Roberto Kolter. Flagellar and twitching motility are necessary for pseudomonas aeruginosa biofilm development. *Molecular microbiology*, 30(2):295–304, 1998.

Supplementary Table

Strain	**Reference**
P. aeruginosa PA14	[65]
rhlA^{-}	[31]
rhlA^{-} *pBAD-RhlAB*	[31]
flgK^{-}	[66]

Table S1: Strains used in this study

Supplementary figures

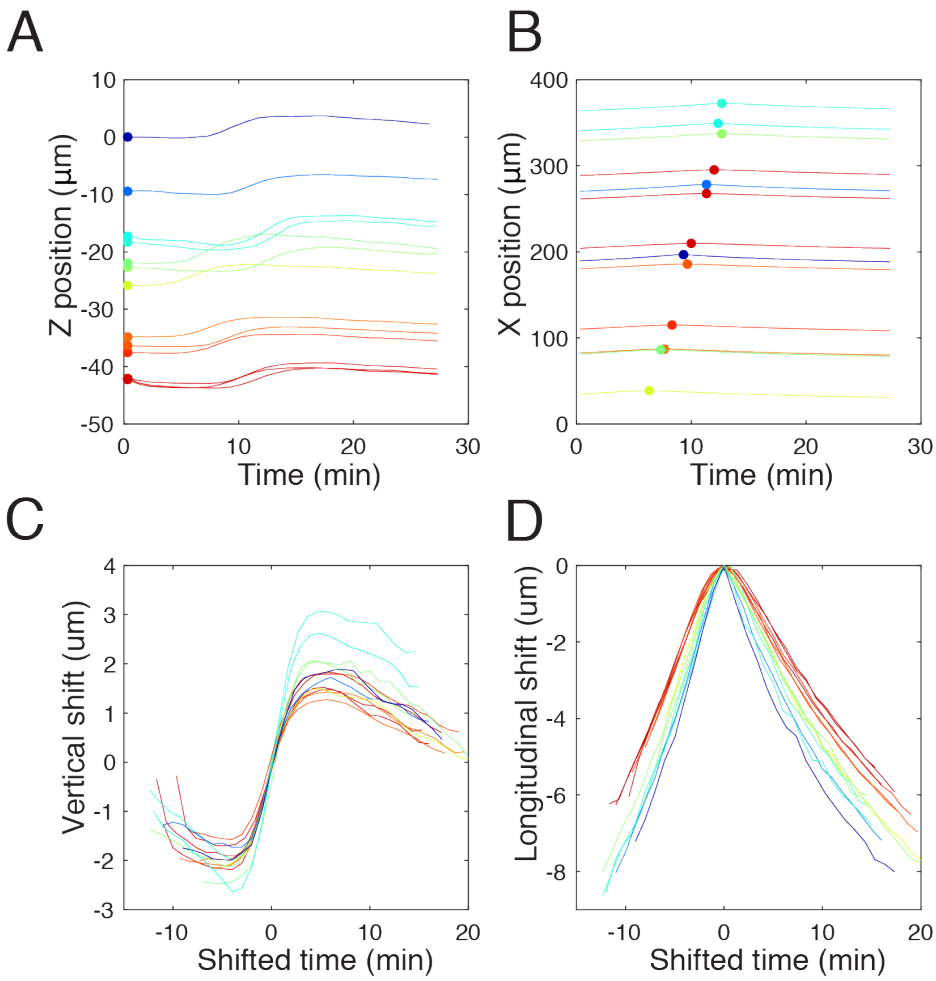

Figure S1: The swelling front is characterized by vertical shift and longitudinal dilation. A: Absolute position $Z(t)$ for all beads (N=13) detected and tracked during this acquisition. Color in all panels codes for initial depth in the gel. B: Absolute position $X(t)$ for all beads. The maximal X position for each bead is depicted with a dot. The (X_{max}, t_{max}) coordinates of these dots reveals the propagation speed of the swelling front. C: Relative vertical positions $(Z(t) - Z(t_{max}))$ for all beads, as a function of relative time $(t - t_{max})$. The swelling amplitude is independent on the initial depth. D: Relative longitudinal positions $(X(t) - X_{max})$, as a function of relative time $(t - t_{max})$. Deeper beads move slower in the longitudinal direction. For the sake of clarity, Figure 2F only represents a subset of the data.

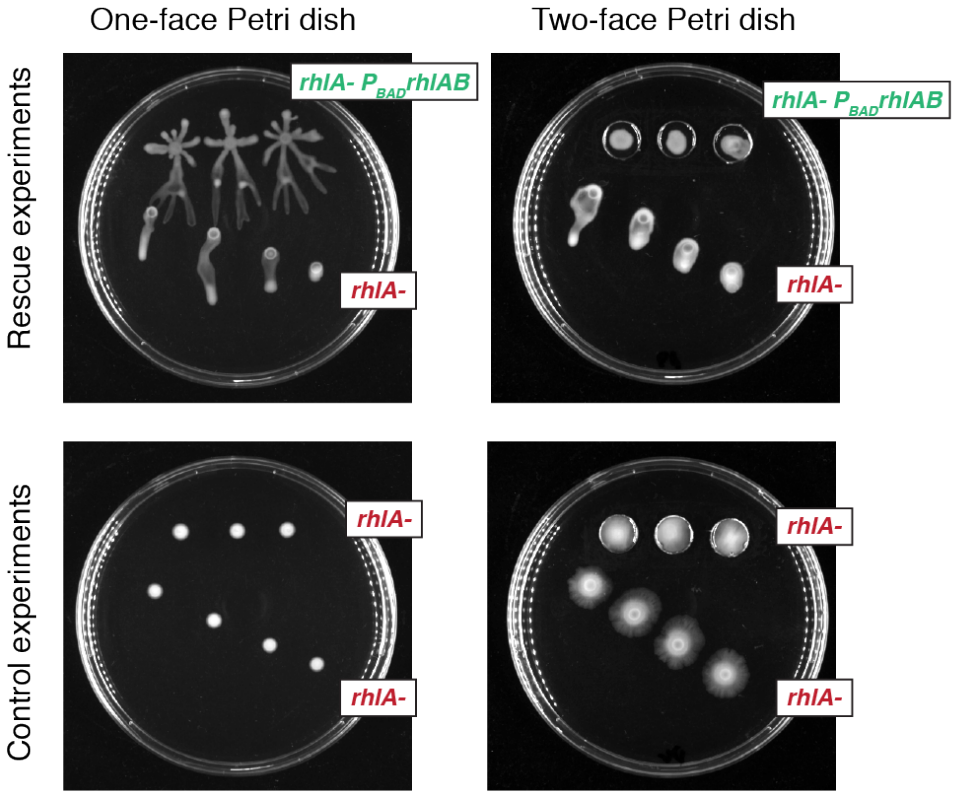

Figure S2: Rescue experiments (top) and control experiments (bottom). Left: on one-face Petri dish. Right: on two-face Petri dish. *rhlA*$^-$ colonies are unable to swarm by themselves. They are rescued using rhamnolipids provided by *rhlA*$^-$ *pBAD-RhlAB* colonies. When facing another *rhlA*$^-$ colony, they are not rescued. Snapshots were taken 15 hours after inoculation for one-face Petri dish, 36 hours after inoculation for two-face Petri dish.

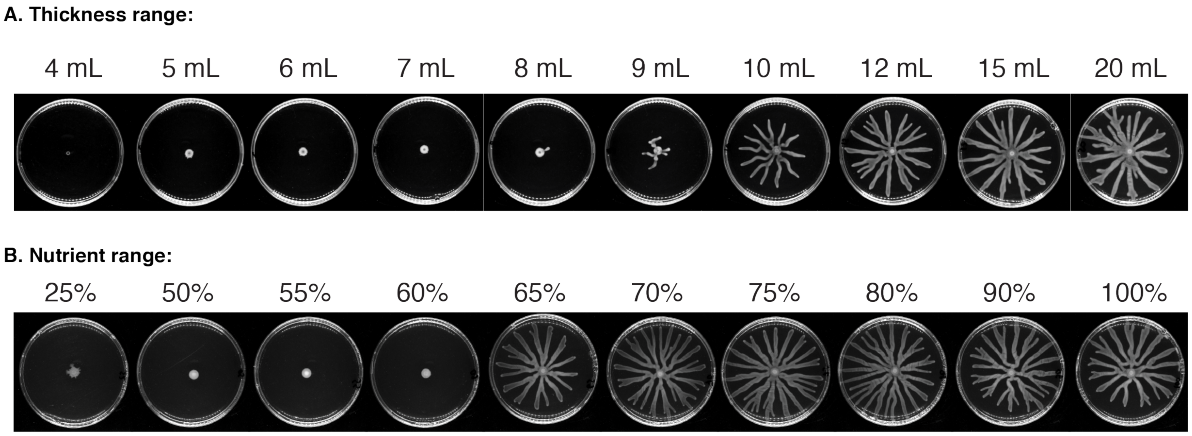

Figure S3: A: Snapshots of swarming colonies grown on gels of various thickness, expressed as volume of agar gel in the plate. 20 mL is the nominal volume, and corresponds to a thickness of 3.5 mm. B: Snapshot of swarming colonies grown on a gel containing various concentration of nutrients (casa-aminoacids). The nominal concentration is 12.5 g/L. Concentrations are expressed as a percentage of this nominal concentration. Note the change of final colony size is abrupt between 60% and 65% concentrations of nutrients, while the change is more gradual between 8 mL and 12 mL volumes. All snapshots were taken 22 hours after inoculation.

Supplementary Movies

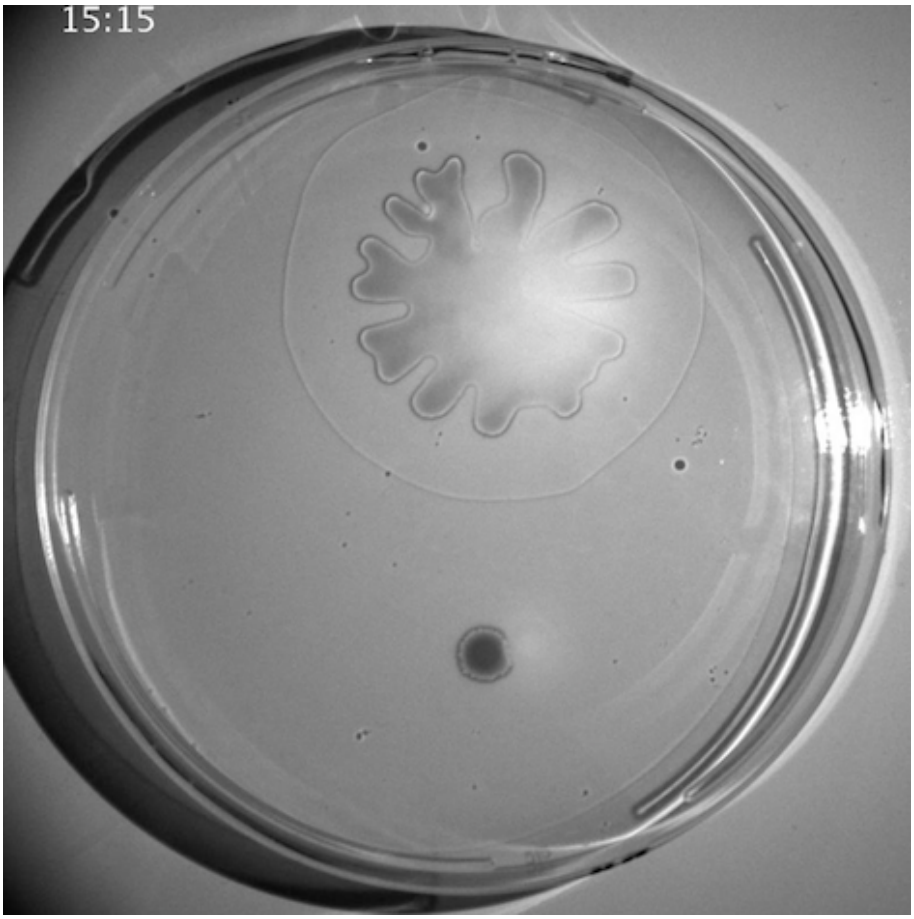

Movie 1: WT vs DR shadowgraphy

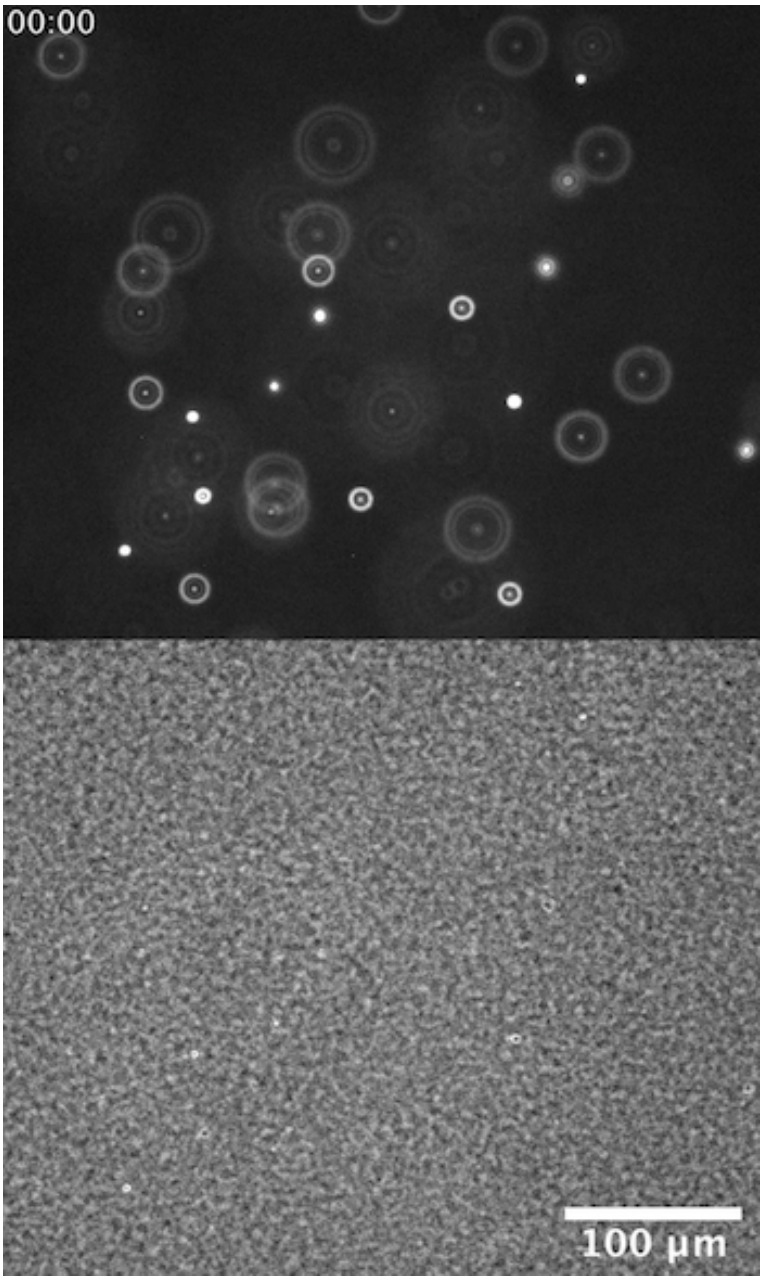

Movie 2: Timelapse video of 1 µm fluorescent beads embedded into the agar gel. Top: fluorescence image. Bottom: phase contrast image. The swelling front passing in the field of view (from left to right) is visible as a white halo in the phase contrast image, from t=4 min to t=15 min.

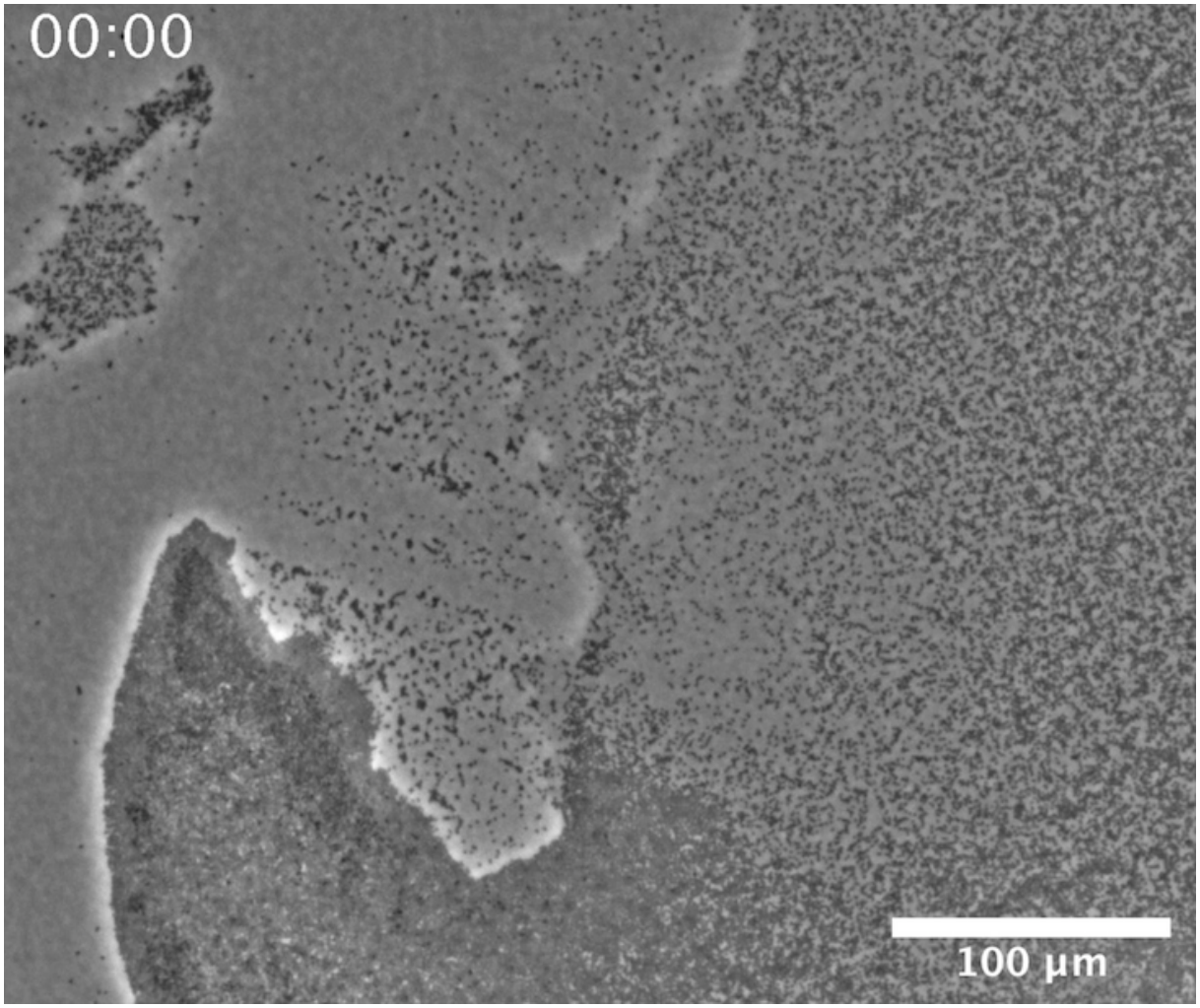

Movie 3: Timelapse video of *rhlA*$^-$ cells motility on agar gel. The swelling front passes through the field of view at t=20 min, from the left side to the right side.

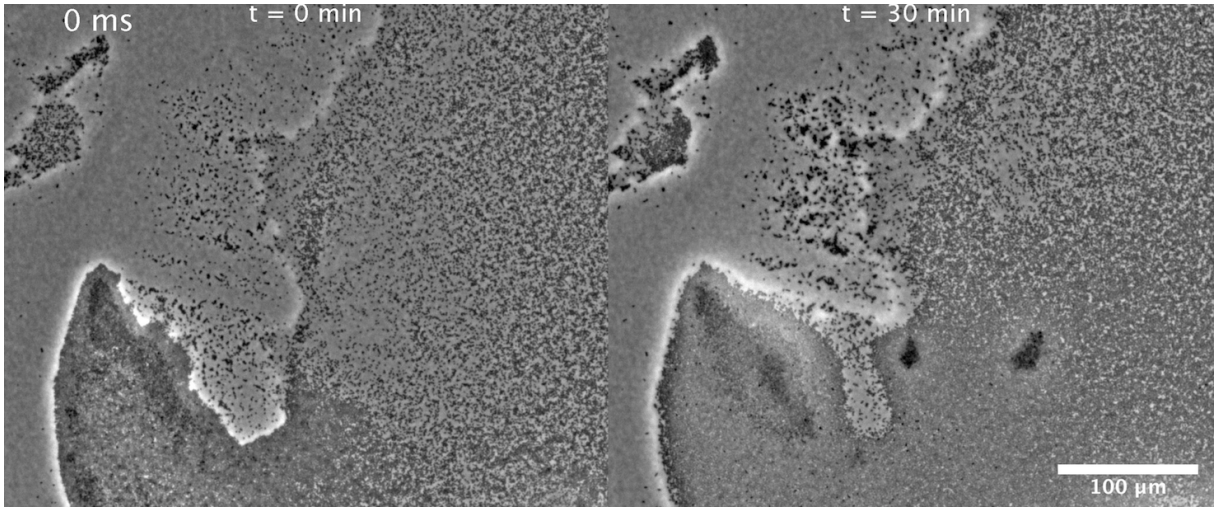

Movie 4: One second long videos of *rhlA*$^-$ cells motility on agar gel. Left: t=0 min, before passage of the swelling front. Right: t=30 min, after passage of the swelling front.

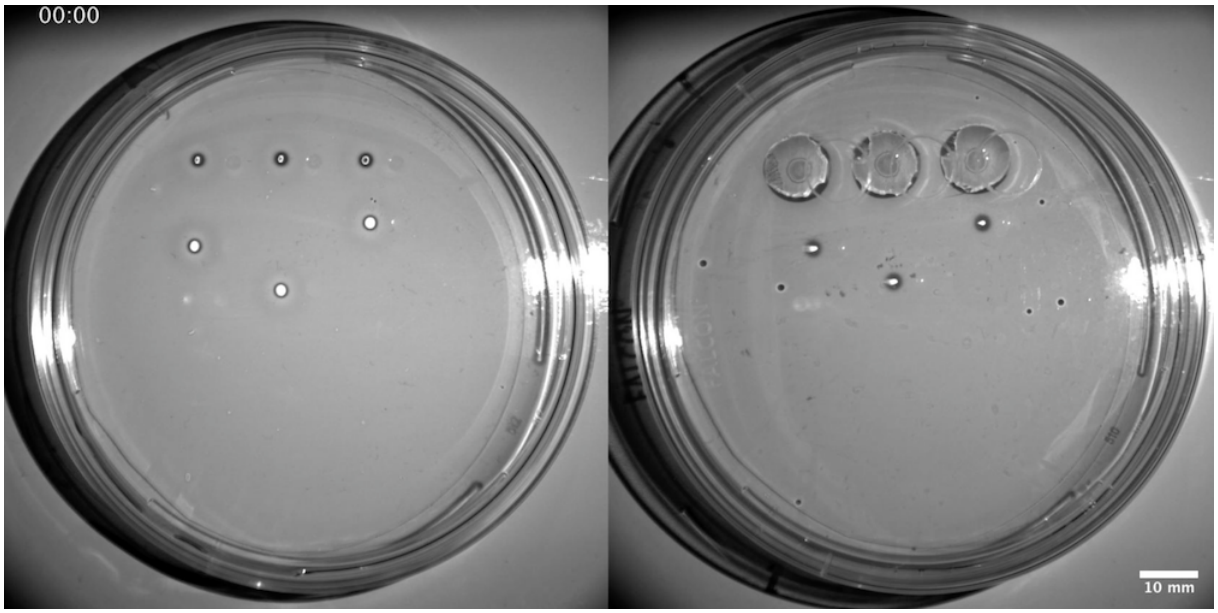

Movie 5: Left: Rescue experiment on a regular one-face swarming plate. Right: Rescue experiment on a two-face swarming plate. In both cases, three *rhlA*$^-$ colonies, unable to swarm by themselves, are rescued using rhamnolipids provided by three *rhlA*$^-$ *pBAD-RhlAB* colonies grown at a distance (ranging from 7 to 23 mm). On the two-face plate, *rhlA*$^-$ *pBAD-RhlAB* colonies are grown on the second face, within holes. On the one-face plate, *rhlA*$^-$ *pBAD-RhlAB* colonies are grown on the same face as the *rhlA*$^-$ colonies. Note that the left and center *rhlA*$^-$ colonies start swarming before the *rhlA*$^-$ *pBAD-RhlAB* colonies reached them (respectively 90 minutes and 140 minutes). Full movie duration is 20 hours.